SLEEP, 2022, 1–14

https://doi.org/10.1093/sleep/zsac132
Advance Access Publication Date: 6 June 2022
Original Article

ORIGINAL ARTICLE

The space-time profiles of sleep spindles and their coordination with slow oscillations on the electrode manifold

Paola Malerba[1,2,*], Lauren Whitehurst[3] and Sara C. Mednick[4]

[1]Battelle Center for Mathematical Medicine, The Research Institute at Nationwide Children's Hospital, Columbus, OH, USA, [2]School of Medicine, The Ohio State University, Columbus, OH, USA, [3]Department of Psychology, University of Kentucky, Lexington, KY, USA and [4]Department of Cognitive Science, University of California Irvine, Irvine, CA, USA

*Corresponding author. Paola Malerba, Battelle Center for Mathematical Medicine, The Research Institute at Nationwide Children's Hospital, 575 Children's Crossing, Columbus, OH 43215, USA; School of Medicine, The Ohio State University, Columbus, OH, USA. Email: malerba.2@osu.edu.

Abstract

Sleep spindles are important for sleep quality and cognitive functions, with their coordination with slow oscillations (SOs) potentially organizing cross-region reactivation of memory traces. Here, we describe the organization of spindles on the electrode manifold and their relation to SOs. We analyzed the sleep night EEG of 34 subjects and detected spindles and SOs separately at each electrode. We compared spindle properties (frequency, duration, and amplitude) in slow wave sleep (SWS) and Stage 2 sleep (S2); and in spindles that coordinate with SOs or are uncoupled. We identified different topographical spindle types using clustering analysis that grouped together spindles co-detected across electrodes within a short delay (±300 ms). We then analyzed the properties of spindles of each type, and coordination to SOs. We found that SWS spindles are shorter than S2 spindles, and spindles at frontal electrodes have higher frequencies in S2 compared to SWS. Furthermore, S2 spindles closely following an SO (about 10% of all spindles) show faster frequency, shorter duration, and larger amplitude than uncoupled ones. Clustering identified Global, Local, Posterior, Frontal-Right and Left spindle types. At centro-parietal locations, Posterior spindles show faster frequencies compared to other types. Furthermore, the infrequent SO-spindle complexes are preferentially recruiting Global SO waves coupled with fast Posterior spindles. Our results suggest a non-uniform participation of spindles to complexes, especially evident in S2. This suggests the possibility that different mechanisms could initiate an SO-spindle complex compared to SOs and spindles separately. This has implications for understanding the role of SOs-spindle complexes in memory reactivation.

Statement of Significance

To understand spindle's role in cognition, it is essential to understand how they organize in space-time, and in relation to slow oscillations (SOs). We describe spindle properties across the scalp, comparing light and deep sleep, and identify five different spindle space-time profiles and their properties. We found Frontal-Right spindles and Posterior spindles, but also Left, Local, and Global spindles. We also found that spindle frequency, amplitude, and duration are different among these types, and that events that coordinate SO and spindle occurrence tend to preferentially involve Global SOs (previously identified with the same method) and Posterior spindles at central locations. This suggests that mechanisms eliciting an SO-spindle complex recruit specific topographic subtypes of events, hence is potentially different from mechanisms initiating spindles and SOs independently.

Key words: sleep EEG; brain oscillations; posterior spindles; global SOs; memory reactivation

Submitted: 4 January, 2022; **Revised:** 19 May, 2022

Graphical Abstract

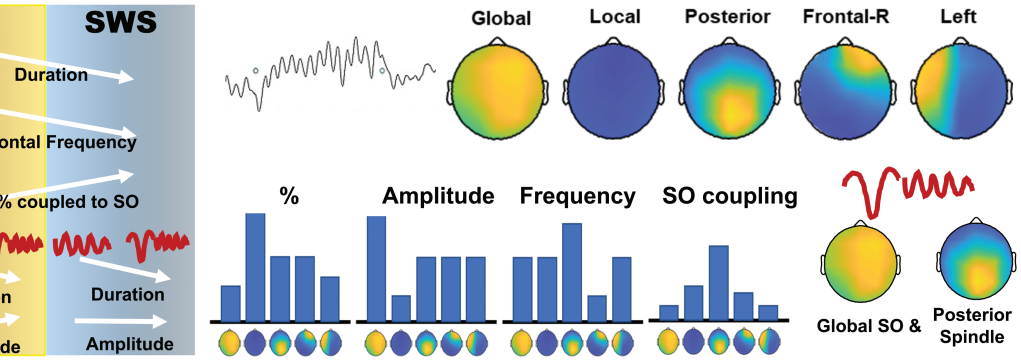

Introduction

Brain oscillations, transient organization of neural activity in distinct frequency bands [1–3], have been linked to behavior, with their emergence and coordination across structures hypothesized to be relevant to cognitive processing [4, 5]. Rhythms have been shown to mediate information processing in various contexts (memory encoding and retrieval, attention, movement initiation, and perceptual binding), and different mechanistical roles for rhythms have been proposed, such as organizing preferential phases of activation (windows of opportunity) for principal cell activity [6–8] or pacing spiking dynamics to promote spike-time dependent plasticity [9–12].

Brain rhythms that emerge during non-rapid eye movement (NREM) sleep cover a range of topographical regions, frequencies, and time scales, including cortical slow oscillations (SOs) [13], cortico-thalamic spindles, [14, 15] and hippocampal sharp-wave ripples [16] (150–250 Hz). Occasionally, these rhythms coordinate in time, where the faster rhythms (spindles and ripples) are nested in specific phases of slower rhythms (SOs) [17–20]. Sleep rhythms have been functionally connected to the restorative nature of sleep [2, 21], homeostasis, [22–24] and consolidation of memory [25–28]. In particular, experiments in humans and animals have shown that altering the presence and coordination of sleep rhythms results in altered memory performance [29–33], where the reciprocal timing of rhythmic activation across brain structures is thought to allow for the appropriate selective reorganization of synapses when supporting reactivation of memory engrams across brain regions [26]. Recent data support an essential role for spindles and their coordination with SOs in supporting hippocampal-dependent memory consolidation, as well as the timing of memory reactivation [11, 18]. However, a mechanistic understanding of how these sleep oscillations support/mediate brain communication is still not complete.

Mechanistically, spindles are understood to be paced by thalamic inhibitory-excitatory circuits [34–36], with their emergence as cortical events shaped by thalamo-cortical circuitry [37, 38], showing high variability, including in their space-time appearance [39, 40]. In the literature, spindles have been shown to vary in frequency (both along the frontal-parietal axis [41–43] and across individuals [39]), propagation paths as local travelling waves (spiraling vs expanding [44]), and in their coordination across cortical layers [45]. The potential relevance of fine spindle space-time propagation patterns to understanding their contribution to cognition is currently under-explored.

In sleep health, spindles are often interpreted as promoting sleep stability by contrasting potential waking factors arising externally (see [46] and [47], but also see [48] for a different interpretation). They are described as symmetric events after the age of 5–6 years [49] and their basic properties, such as density and fronto-parietal emergence, have been linked to age [50–52], average intelligence [53–56], and hormonal phases [57–59]. While cognitive and health-focused studies of sleep emphasize the functional importance of spindles, the potential role of changes in spindle space-time patterning as biomarkers in development and hallmarks of changes in brain dynamics that underlie cognitive symptoms emerging in clinical populations is strongly understudied.

Describing and understanding spindle patterning on the scalp in a data-driven way is a crucial step in establishing standardized methodologies to evaluate functional quantifiers as potential biomarkers in typical and clinical populations. It is also essential to initiate the process of embedding our understanding of time-based coordination of SOs and spindles into a space-time-based coordination framework. This is necessary to the development of exhaustive mechanistic models of spindles' role in cognitive processes.

In this study, we set out to classify spindle space-time profiles with a data-driven clustering approach that we have previously developed to examine SOs [60]. In this approach, single events are detected independently across electrodes and their co-occurrence within a short time delay is encoded in a binary matrix that can be clustered with balanced algorithms. Furthermore, we investigated the coordination between spindle and SOs in relation to the space-time profiles of both SOs and spindles. We begin by studying the basic properties of spindles detected using a broad frequency range (10–16 Hz), and compare density, duration, amplitude, and frequency of spindles that occur at short delays from SOs to those of spindles that occur independently of SO timing, and in SWS vs S2 sleep. We then extend our topographical classification method, originally applied to SOs, to spindles. We find five topographical types of spindles that are present in both S2 sleep and SWS. Based on their scalp concentration we label them Global, Local, Posterior, Frontal-Right, and Left spindles. In parallel with our findings on SOs, Global spindles have largest amplitudes, and Local spindles have smallest amplitude of all types in both stages. At centro-parietal locations, Posterior spindles have faster frequency than other spindle types, and show longer duration (albeit only in S2 sleep).

When grouping complexes of SOs and spindles depending on SO type (Global, Local, or Frontal) and spindle type, we are able to compare how frequently each possible combination occurs at different scalp locations. We find that while space-time clustering does not distinguish coupled and uncoupled spindles in different groups, the most common type of SO-spindle complex involves a Posterior spindle occurring right after the down-to-up transition of the Global SO, detected on the central region of the scalp during SWS. Hence, there is a non-uniform involvement of spindles in coupling with SOs, suggesting that mechanisms that lead to the emergence of complexes of one SO and one spindle selectively recruit specific space-time profiles.

Methods

Sleep acquisition and staging

One night of sleep was recorded in 34 subjects (18 females). EEG data were collected with BrainVision acquisition system and a 32-channel cap (EASYCAP GmbH) with Ag/AgCI electrodes placed according to the inter-national 10–20 System (Jasper, 1958). Twenty-two out of 32 electrodes were passive scalp recordings. The remaining electrodes were used for electrocardiogram (ECG), electromyogram (EMG), electrooculogram (EOG), ground, an online common reference channel (at FCz location, retained after re-referencing) and mastoid (A1 and A2) recordings. The EEG was recorded with a 1000 Hz sampling rate and was re-referenced to the contralateral mastoid (A1 and A2) post-recording. High-pass filters were set at.3 Hz and low-pass filters at 35 Hz for EEG and EOG. Eight scalp electrodes (F3, F4, C3, C4, P3, P4, O1, and O2), the EMG and EOG were used in the scoring of the nighttime sleep data. Raw data were visually scored in 30-second epochs into wake, stage 1, stage 2 (S2), SWS, and rapid eye movement sleep (REM) according to the Rechtschaffen and Kales' (1968) manual. Note that we increased the electrode count compared to standard method to enhance scoring reliability, but did focus on the output from the C3 and C4 electrodes. Minutes in each sleep stage were calculated. Additionally, wake after sleep onset (WASO) was calculated as total minutes awake after the initial epoch of sleep. The outcome of scoring across all subject has been previously reported [60].

Spindle Detection Algorithm

Our custom-designed spindle detection algorithm builds on many known spindle properties, including frequency range [61], waxing-waning profile, and local sigma prominence in a time window nearby a detected spindle (given spindles happen with some refractory period between them [62]). Detection is performed in each EEG channel separately. Detection was only performed in epochs scored as S2 and SWS, and focused on times that were artifact-free, where artifactual times were marked directly after sleep scoring and prior to spindle detection. Data was filtered between 9 and 16 Hz (Butterworth, band-pass filter of order 6) taking care to not introduce shifts in the time series (using *filtfilt* function in MATLAB). The root-mean square over 100 ms epochs of the filtered channel was calculated in 30-second-long epochs, which were then z-scored. Within such 30-second-long z-scored time series, peaks with minimal prominence of 0.5 and minimal height of 3.5 were detected. This implies that we looked for sigma peaks (consistent with recently proposed approaches [15, 39]) that were at least 3.5 standard deviations larger than the 30 seconds mean, and with local prominence of at least 0.5 standard deviation within those 30 seconds. Each peak found in the sigma-filtered signal by this algorithm located a putative spindle. For each putative spindle that was found during either one of the sleep stages of interest (S2 or SWS), we isolated a time epoch 1 second before and 1 second after the putative spindle peak. The original channel data for such time epoch was high-pass filtered at 0.006 Hz to eliminate ultra-slow drift interference in subsequent evaluations, again using a Butterworth filter of order 6 removing shifts. The Morlet Wavelet spectrum for this 2-second-long epoch was calculated using function *cwt* in MATLAB. This time-frequency-power representation was then used to find peak time, start, and end time and dominant frequency of the spindle event. To do this, 20 level curves were isolated in the time-frequency plot around the putative spindle peak. Closed loops in the level curves who had centers with y-coordinate within the frequency range (6–16 Hz), and the x-coordinate within 0.5 seconds of the RMS peak time were considered indicators of the presence of a spindle. If such a loop was found, then all the level curves concentric to the peak time-frequency point were found, and the level curve that showed half-height in power was used to determine start and end of the spindle (by finding the times that corresponded to the minimum and maximum time included in the level curve, respectively). The level height of the tallest level curve found within the spindle was divided by 20 (the total number of level curves allowed in the complete [–1,1]s interval) to output a confidence index on the detected spindle. Double detections were removed from the list of spindles at this stage. Putative spindles confirmed by this algorithm step were lastly verified by finding the peaks in the original channel trace within the [–1,1] second interval, and if no peaks between the putative start and end point of the spindle were found, the spindle was discarded. Of note, while automatic spindle detection approaches are always evolving and improving, our approach is consistent with the overall methodology of other spindle detectors made available in the literature [15, 57, 63, 64], where data are initially filtered in a sigma band to identify candidate peaks, and the trace in candidate peaks is then evaluated in frequency and amplitude to accept or reject the candidate event. Our approach emphasizes our requirement that the wide-band spectrogram derived from the unfiltered trace nearby a candidate event shows an isolated spindle with persistent frequency (in other words, that power found in the filtered signal was not leaking from nearby frequency bands and that the rhythmic event was not strongly accelerating/decelerating and exiting the sigma band during its duration).

Measuring spindles properties (density, frequency, amplitude, and duration)

Spindle density was measured in each electrode as the count of all spindles found in a given sleep stage (S2 or SWS) across the night divided by the time (in minutes) spent in the sleep stage across the whole night. As such, this is a fundamentally stationary measure. The frequency of each spindle was identified from the spectrogram taken in a 2-second-long time interval around the whole spindle event, where the tallest level-curve

in the time-frequency-power representation (i.e. the ellipse with the highest power in the sigma range around the spindle) was identified, and the frequency value at the center of such ellipse marked the spindle frequency. Spindle duration is the time (in seconds) elapsed between spindle initiation and end. Spindle amplitude is found as the largest voltage in the spindle signal filtered between 9 and 16 Hz with an order 6 Butterworth band-pass.

Spindle clustering on the electrode manifold

This method focuses on first detecting spindles at each given electrode separately. Then, for each detected spindle, identifying which other electrodes also had a spindle event within a short time delay. This allows for the creation of a binary array (a 0 or a 1 value for each electrode) for each spindle, or a binary matrix when listing all available spindles. K-means clustering applied to the binary matrix using Hamming distance allows for identification of spindles that show similar topographies at small delays. Specifically, consistent with our approach in ref. [60], we apply k-means in Matlab with 200 replicates and a maximum iteration of 10,000 with the option of dropping empty clusters and preserving the default setting of adaptive initialization with kmeans++. The algorithm identifies centroids as well as cluster assignments for each spindle event. This is performed separately for S2 and SWS spindles.

In this study, we used a time delay of 300 ms to build the binary matrix. This time delay was chosen to allow for co-detected spindle peaks to occur within the duration of the spindle of reference. Methodological considerations on a range of delays (shown in Supplementary Figure S2) were made, and 300 ms showed a different spindle footprint in S2 compared to SWS, which informed our choice.

To make a principled decision about how many clusters to use (spindles are very localized objects, it can be hard to make an a-priori decision) we look at the changes in overall distance from centroid that we obtain applying clustering with different cluster numbers. The slope of the decreasing graph that maps cluster count to overall distance from centroid was shallower (i.e. a plateau range begins) starting with $k = 5$. This meant that adding more clusters up to a count of 5 changed the overall distance from centroid strongly, but that degree of change became small for cluster counts above 5. Hence, we chose to use 5 clusters.

SO detection

To detect the presence and timing of each SO event in any given electrode, we first applied a detection algorithm which we used in our previous work [60] and closely followed the criteria introduced by Massimini et al.[13], and was initially introduced in Dang-Vu et al. [65]. The following description matches the one reported in methods in ref. [60]. In short, the EEG signal was filtered in the 0.1–4 Hz range, and candidate portions of the signal between subsequent positive-to-negative and negative-to-positive were listed as possible SOs. These events were only considered SOs if the following criteria were satisfied: (1) the wave minimum was below or equal to 80 uV, (2) the range of values between maximum and minimum voltage was at least 80 uV, (3) the time between the first and second zero crossing in the data had to be between 300 ms and 1 second, and (4) the total duration of the candidate event was at most 10 seconds. The pool of candidate SO events satisfying the parameters were further screened to remove potential artifacts, by computing the amplitude at trough referenced to the average of the signal ±10 seconds around the minimum. Events at one electrode which showed an amplitude size of 4 SDs above the mean of all events detected at that electrode were discarded, and a secondary distribution of amplitudes including all events from all electrodes of a subject was created, and again events with amplitude above 4 SDs from the mean were discarded. When selecting the SOs happening during a given sleep stage (S2 or SWS), only SOs with beginning and end included within the sleep stage were considered. Details on specific properties of detected SOs, including amplitude, duration, and density, are reported in ref. [60].

Statistical analysis

When comparing spindle properties statistically, we computed the average value of interest for each participant and populated a by-participant table organized based on factors of interest. In Figure 1B and C, repeated-measures ANOVA was used in B–C to study the effect of sleep stage and electrode on the dependent variable (spindle density, duration, or frequency). Post-hoc pairwise analysis was performed with Wilcoxon signed-rank test, concentrating on comparing the two sleep stages within any given electrode. Bonferroni corrections were used to assess significance.

In all panels in Figure 2A, we used two-way repeated-measures ANOVA to compare the percent of events (dependent var) across both electrodes and type of complex (e.g. SO-SP* and SP*-SO) (independent vars). Post-hoc analysis (Wilcoxon signed-rank test) tested which electrode-by-complex cases were statistically significantly larger than others. Bonferroni corrections were used to assess significance.

In all panels in Figure 2B–D, we used two-way repeated-measures ANOVA to compare the spindle property (e.g. frequency for Figure 2B left panel) (dependent var) across both electrodes and type of complex (SO-SP*, SP*-SO, and All SPs) (independent vars). Post-hoc analysis (Wilcoxon signed-rank test) tested which electrode-by-complex cases were statistically significantly larger than others. Bonferroni corrections were used to assess significance.

In Figure 3B, we used a two-way repeated-measures ANOVA to compare the fraction of SPs (dependent var) across both cluster type and sleep stages (independent vars). Bonferroni corrections were used to assess significance. In the post-hoc analysis, we tested the effect of sleep stage with Wilcoxon signed-rank test, Bonferroni corrected.

In Figure 3C, for each panel, we used a two-way repeated-measures ANOVA to compare each SP property (dependent var) across both electrodes and type of cluster (independent vars). Bonferroni corrections were used to assess significance. In the post-hoc analysis, we tested the effect of cluster type and electrode with Wilcoxon signed-rank test, significance was Bonferroni corrected.

Results

Different spindle properties in S2 vs SWS

Focusing on stage 2 sleep (S2) and slow wave sleep (SWS) separately, we leveraged the time-frequency profile of the EEG

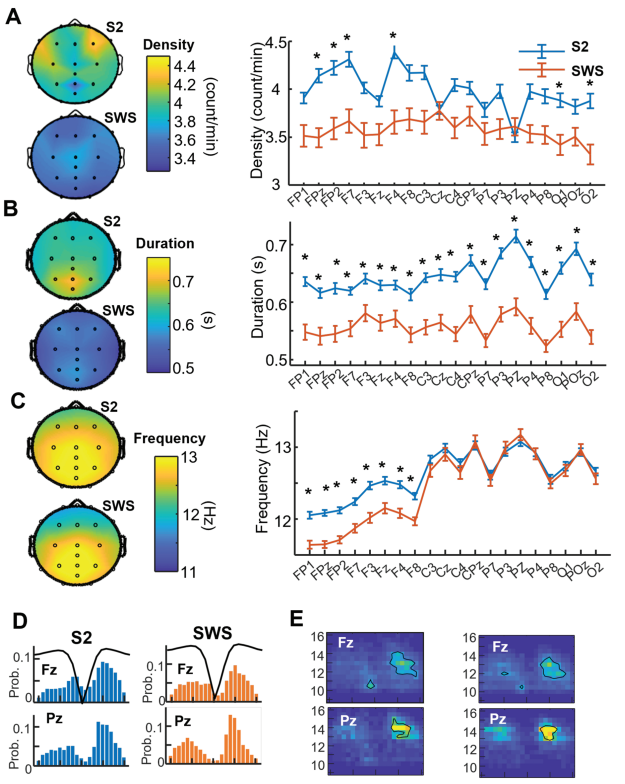

Figure 1. Basic properties of spindles in SWS vs S2. (A–C) Spindle properties in S2 and SWS, shown in topoplots (left) and value-by-electrode plots (right). In all these line plots, error-bars are SEM across the 34 participants. Stars represent statistically significant difference in the variable value at the two sleep stages within a given electrode (see Methods and Results). Average density (count per minute) of spindles (A). Average duration (in seconds) of spindles (B). Average frequency (in Hz) of spindles (C). (D) Sample probability of spindle detection within one second of a SO trough. For each electrode, we consider each detected SO, and the time interval including 1s before and after the trough, in 100-ms-long bins. We count how many spindles are found in each bin and divide by all the spindles found within that time interval, to obtain a probability density distribution (this implies that we ignore all the spindles which do not happen nearby a SO trough in these distributions). The final plots show the average distributions across all subjects. Left column shows S2, right column SWS, at Fz and Pz electrodes. Note that timing of spindles around SO troughs is more sharply organized posteriorly than frontally. (E) Probability of spindle timing and frequency within a second of a SO trough. Using the same timing procedure as in D, we also separate spindles based on their frequency, in 1 Hz-wide bins. This creates a two-dimensional sample probability density. The final plots show the average distributions across all subjects. Left column shows S2, right column SWS, in electrodes Fz and Pz.

signal to detect spindles at each electrode, and determined their start and end times, frequency, and amplitude (see Methods). Consistent with our expectations, we found a larger spindle density (count per minute) in S2 compared to SWS (Figure 1A), (with an effect of sleep stage, electrode, and interaction; post-hoc analysis found statistical difference among sleep stages at some frontal and occipital electrodes, shown with stars; see Methods - Statistical Analysis). Spindle amplitude was slightly larger at frontal electrodes and did not differ between the two sleep stages (Supplementary Figure S1A), however, its relation to frequency had different profiles in S2 vs SWS (Supplementary Figure S2A).

We also found that spindles lasted about 100 ms longer (on average) in S2 compared to SWS (Figure 1B). Statistical analysis found an effect of sleep stage, electrode, and interaction; with post-hoc analysis showing statistical difference among all electrodes across sleep stages (see Methods - Statistical Analysis). This difference in duration was not due to a rigid shift of the distribution of spindle duration toward higher values when comparing SWS to S2 spindles, but rather by an increased relative presence of relatively long spindles (about 1 second long) in S2 compared to SWS (Supplementary Figure S1B), driving the mean of the distribution toward higher values.

Spindle frequency showed a continuous increase from frontal to parietal regions (Figure 1C). Interestingly, there was a frequency differentiation between S2 spindles and SWS spindles at frontal electrodes, where S2 spindles appeared slightly faster than SWS spindles (statistical analysis found an effect of sleep stage, electrode, and interaction; with post-hoc analysis showing statistical difference among sleep stages only at frontal electrodes; see Methods - Statistical Analysis). The separation of spindle frequency frontally and not parietally, combined with the increase in frequency from frontal to parietal regions, is consistent with common nomenclature of fast and slow spindles being found parietally and frontally, respectively [39, 42, 66, 67]. However, at all electrodes we found spindles of frequencies across the available range (10–16 Hz, Supplementary Figure S1C); and the average spindle frequency differed only of about 1 Hz between frontal and parietal electrodes in our data.

We then asked if our data supported the temporal coordination of spindle/SO coupling found in the literature [18, 68–70]. For each SO detected at each electrode [60], we considered a time interval of 1 second preceding to 1 second following the SO trough and, if a spindle peak was detected within that interval, we logged its time. This produced a sample distribution histogram of spindle timing referenced to SO trough at each electrode (Figure 1D and Supplementary Figure S2B). In both S2 and SWS, data showed two preferential time delays for spindle occurrence nearby an SO trough: about 500 ms preceding and 500 ms following the trough. However, these two windows of opportunity were differently shaped, with the preceding peak (500 ms before SO trough) being broad and shallow, indicating low time specificity, at all electrode locations. Conversely, the following peak (500 ms after SO trough) showed a sharp peak, which narrowed from frontal to parietal regions. The sharpness of the post-trough peak is consistent with ideas that consider the SO trough capable of initiating a coordination of local cortical activity and thalamo-cortical activation [17, 71–73].

Next, we examined if spindles coupled with SOs share common features. We thus populated a two-dimensional sample probability distribution plot for each electrode, in which we considered the timing aligned to an SO trough on the horizontal axis and the spindle frequency on the vertical axis (Figure 1E and Supplementary Figure S2C). Color in each location would show uniform vertical bars if there was no special frequency selectivity of spindles coordinating with SOs. In particular, if frequency was not a factor, the vertical bars would look similar preceding or following the SO. Once again, data showed a specific selectivity in spindle time that favored a delay of about 500 ms after the SO trough. The spindles that demonstrated this temporal preference could often be characterized in a narrow frequency range of 13–14 Hz. This was especially evident in SWS, and in centro-parietal electrodes. Of note, data in Figure 1E also show a light shadow of fast frequency spindles preceding the SO trough in SWS at centro-parietal electrodes. We hypothesize that this could be an effect of trains of SOs (more common in SWS compared to S2), in which a spindle that followed one SO trough also is counted as preceding the subsequent SO trough.

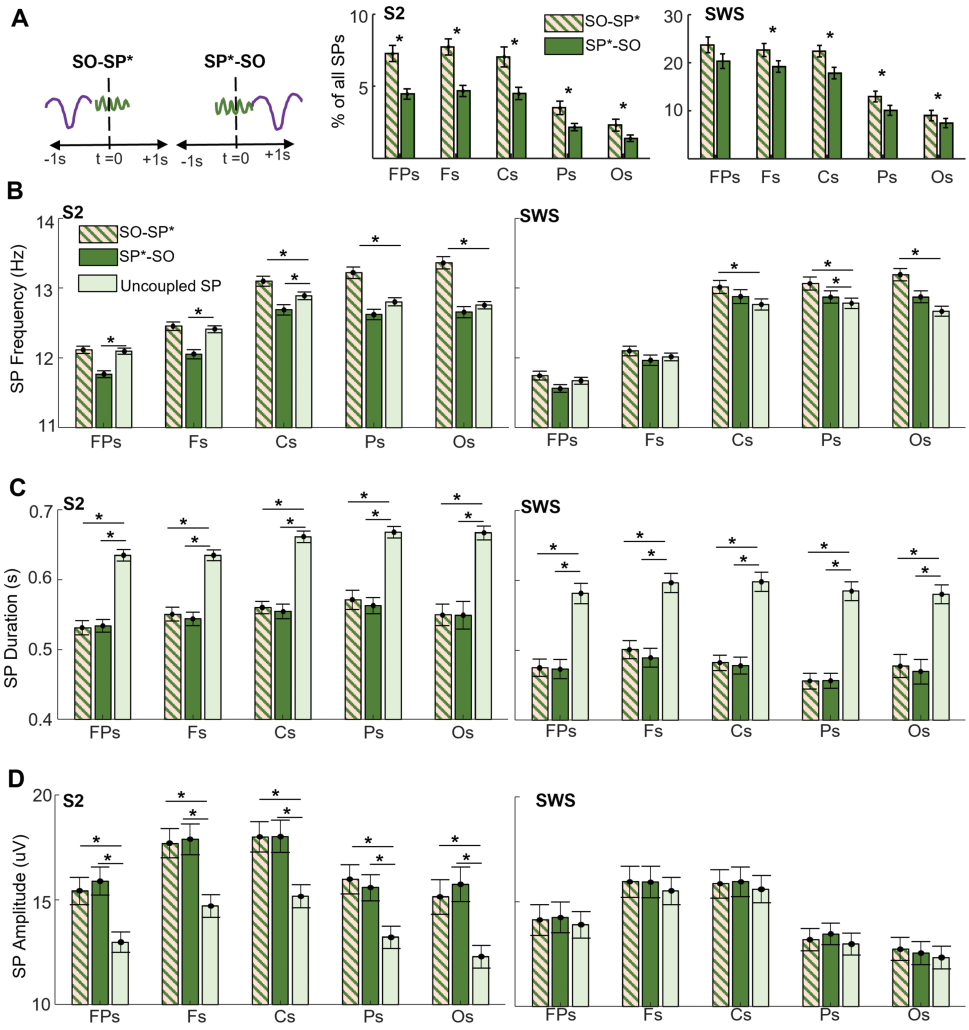

Figure 2. A minority of spindles and SOs is involved in SO-spindle complexes. (A) Counting events that combine one SO and one spindle, referenced to the peak of the spindle (time 0). Left plot: A graphics representation of the proposed nomenclature: SO-SP* complexes are a combination of first detecting one spindle and then finding one SO in the second preceding the spindle peak, while SP*-SO complexes are a combination of first detecting one spindle and then finding one SO in the second following the spindle peak. Middle and Right plot: Percent of all detected spindles (SPs) during S2 or SWS that are part of an SO-SP* complex or an SP*-SO complex. Error bars mark SEM across subjects. (B) Spindle frequency (in Hz) across locations on the electrode manifold. Compared are three groups: all spindles found in a chosen sleep stage (S2 is to the left, SWS to the right), the sub-group of those spindles that are part of an SO-SP* complex (striped bar) and the sub-group of all spindles that are part of an SP*-SO complex. (C) Same as A, but for spindle duration (measured in seconds). (D) Same as A, but for spindle amplitude (measured in uV).

In summary, our data in Figure 1 suggest that differences between S2 and SWS spindles go beyond spindle density. S2 spindles also show longer duration, faster frequency at frontal electrodes and more frequency–amplitude selectivity at centro-parietal electrodes than SWS spindles. However, the time-based coordination between spindle and SOs appears similar in the two sleep stages.

Properties of spindles in SO-spindle complexes

Our data confirmed that the temporal coordination of spindle and SO complexes show a spindle frequency selectivity. Conceptually, it is common to interpret SO-spindle complexes as SO-driven events. However, most evidence suggests that the presence of an SO, even a large-amplitude one, such as a Global SO, does not automatically induce a spindle. In fact, the majority of SOs do not coordinate with a spindle at all. As such, we were interested in testing if spindles that participate in complexes and "uncoupled" spindles showed structural differences. We chose to analyze these differences as comparison in fundamental properties of spindles, comparing spindles that precede or follow SOs at short delays (within 1 second), to spindles that occur with no SO detected at the same electrode in the same delay, which we label uncoupled. This is driven by our interest in understanding what causes a spindle showing a specific space-time profile to emerge at a given moment and scalp location (say linked to SO timing or not). To eventually achieve that goal, it is crucial to establish how often a given SO is likely to be followed by a spindle, or a given spindle is likely to emerge following an SO. While the two ideas coincide when measuring timing of SO and SP to find SO-SP complexes, they do not coincide conceptually as mechanistic events. For ease of notation, we marked with an asterisk (*) which event (SO or spindle, SP) in the complex is detected as a reference and list the other one as detected either as preceding or following (Figure 2). Thus, an SO*-SP complex is

identified when the detection algorithm is referenced to SO and a spindle occurs in the second after the SO trough; an SP-SO* complex is identified when detection is referenced to SO and a spindle is detected in the second that precedes the SO. In Figure 2A, we give a graphic representation of this nomenclature, for ease of following. It is important to count SO-referenced complexes (SO*) and spindle-referenced complexes (SP*) separately, since we are comparing S2 and SWS and the relative presence of spindles and SOs is drastically different in the two sleep stages, where S2 is rich in spindles and poor in SOs and in SWS the opposite occurs. We report information for SP*-SO and SO-SP* in Figure 2, and for SO*-SP and SP-SO* complexes in Supplementary Figure S3.

In Figure 2A, we concentrate on SP* complexes (SP*-SO and SO-SP*). For different regions on the scalp, from frontal to parietal, we created a "pairing ratio" measure for each category of spindle-SO complex by dividing the count of SPs with an SO preceding (SO-SP* events) or following (SP*-SO events) by the total spindle count in a given sleep stage. As can be seen in the range of the y-axis, we found that a minority of all SP events were participating in complexes, with 5%–10% of all spindles in S2 and 10%–25% of all spindles in SWS detected in either type of complex. When comparing spindles paired to preceding vs following SOs, data showed that in both sleep stages, but most prominently in S2, a greater number of spindles were involved in SO-SP* than in SP*-SO complexes (statistical analysis found an effect of electrode, type of complex, and interaction in Figure 2A for S2, with post-hoc analysis confirming the difference in fraction of SPs involved in SP*-SO vs SO-SP* complexes during S2. In Figure 2A for SWS, statistical effect of electrode, complex type, and interaction was found, with post-hoc analysis confirming the difference in fraction of SPs involved in SO-SP* vs SP*-SO complexes during SWS at all electrodes but FPs).

It is worth observing that if the occurrence of SOs and spindles were completely independent of each other, they could still occasionally be found as complexes by occurring at a short time delay. However, these would be evinced as uniform distributions (rather than peaks) in Figure 1D, no frequency selectivity would be found in Figure 1E and bar heights in Figure 2A would not differ for preceding vs following complexes (e.g. the SO-SP* bar at frontal electrodes would look the same height as the SP*-SO bar). Our data rather support a picture of SO-spindle coordination that includes a majority of spindles and SO occurring independently of each other, and a minority of specifically coordinated spindles and SOs, with spindles of faster frequencies tending to be locked at about 500 ms delay following a SO trough.

In Figure 2B–D, we consider the basic properties (frequency, duration, and amplitude) of spindles that participate in SO-SP* and SP*-SO complexes; and compare them to the average values of these properties in spindles that are not found in close time proximity (±1 seconds) to an SO, which we label uncoupled spindles. Consistent with the rest of our analysis, we compare spindles in S2 and SWS separately. This analysis allows us to test if the minority of spindles that coordinate with SO show specific properties compared to the general spindle population.

Spindles in SO-SP* complexes during S2 (Figure 2B, left panel) had higher frequency than uncoupled spindle frequency at centro-parietal locations, while spindles in SP*-SO complexes showed frequency lower than uncouple spindles at fronto-central locations. (Statistical analysis found an effect of electrode, type of complex, and interaction, with post-hoc analysis confirming the difference in frequency of SO-SP* spindles at C-P-O locations, and of SP*-SO spindles at FP-F-C locations). Frequency of spindles in SO-SP* complexes during SWS (Figure 2B, right panel) was higher than uncoupled spindle frequency at all locations but FPs, while spindles in SP*-SO complexes showed frequency lower than uncoupled spindles at FP locations. (Statistical analysis found an effect of electrode and type of complex but not interaction, with post-hoc analysis confirming the difference in frequency of SO-SP* spindles at F-C-P-O locations, and of SP*-SO spindles at FP locations).

Duration of spindles in either SO-SP* complexes or SP*-SO complexes during S2 (Figure 2C, left panel) was lower than uncoupled spindle duration at all locations. (Statistical analysis found an effect of electrode and type of complex but not interaction, with post-hoc analysis confirming the difference in duration of spindles in either complex type at all locations). The same was true for spindles in SO-SP* and SP*-SO complexes during SWS (Figure 2C, right panel). (Statistical analysis found an effect of type of complex but not electrode or interaction, with post-hoc analysis confirming the difference in duration of spindles in either complex type at all locations).

Amplitude of spindles in either SO-SP* complexes or SP*-SO complexes during S2 (Figure 2D, left panel) was larger than uncoupled spindle amplitude at all locations. (Statistical analysis found an effect of electrode and type of complex but not interaction, with post-hoc analysis confirming the difference in amplitude of spindles in either complex type at all locations). However, no difference was found for spindles in SO-SP* and SP*-SO complexes during SWS (Figure 2D, right panel). (Statistical analysis found an effect of electrode but not type of complex or interaction, with post-hoc analysis negating the difference in duration of spindles in either complex type at all locations).

In summary, our data show that in S2, where spindles are abundant, spindles in complexes (SP*), whether SO-SP*or SP*-SO, are larger and shorter than uncoupled spindles. Furthermore, spindles in SO-SP* complexes (but not those in SP*-SO complexes) are faster in frequency at centro-parietal electrodes. In SWS, where fewer spindles are found, spindles in complexes are still shorter than uncoupled spindles. However, their amplitude is not different from uncoupled ones. While spindles in SO-SP* complexes are slightly faster than uncoupled spindles at centro-parietal electrodes, the difference in frequency is much less pronounced in SWS compared to S2. The selectivity for amplitude and frequency in spindles that participate in complexes of one SO and one spindle, and the difference in the properties of spindles involved in complexes found in S2 compared to SWS, support the concept that SO-spindle complexes are cortico-thalamic events that recruit specific types of SOs and specific types of spindles, as opposed to random occurrences of separately generated rhythms.

Clustering over co-detection reveals five topographical spindle types

Our analysis so far suggested that spindles were highly variable events, with differentiation in their properties and interaction with SO in frontal vs centro-parietal regions. This was consistent with the common interpretation that there are fundamentally two types of spindles: fast spindles detected parietally and slow spindles detected frontally. However, we did find spindles of all frequencies at all electrodes and a gradual

progression of average spindle frequency from frontal to parietal electrodes, and a marked, sleep-stage specific, difference in properties of the minority of spindles involved in complexes with an SO compared to generic spindles. This led us to investigate spindle topography with our clustering over co-detection at a delay technique, which we had introduced for SO analysis [60]. For all spindles detected at one electrode, we measured spindle peak amplitude time and considered a time interval of 300 ms preceding and 300 ms following this peak time (choice of this value is discussed in Methods and Supplementary Figure S4). For each electrode on the scalp, we marked a value of 1 (or "true" in binary logic) if a spindle was also detected at that electrode in the time window. We marked a value of 0 ("false") if no spindle peak was found in the interval. This led us to construct a binary matrix that listed all electrodes (the rows of the matrix) and all detected spindles (the columns). A k-means clustering algorithm was then optimized (see Methods) to choose the number of clusters. We expected about three clusters (a parietal, a frontal and a local), but data showed that five was the minimal number of clusters at which the algorithm plateaued in both S2 and SWS separately. Once we used the five clusters in the algorithm, we looked at their topographical profiles on the electrode manifold by showing the average of detection electrode locations for spindles in topoplots (Figure 3A). We interpreted the different clusters as identifying the following topographical spindle types: Global (co-occurring at a large majority of electrodes), Local (only few non-specific locations), Posterior spindles (co-occurring in the centro-parietal region), Frontal-Right and Left spindles. Of note, we find lateralization in two of the five spindle clusters, which was not an expected outcome. One possible explanation for this lateralization may be that it was induced by our choice of referencing (to the contralateral mastoids, see Methods). However, if referencing was the cause, its effects would be present in all clusters rather than only a minority, in particular that the Posterior cluster could not emerge under that hypothetical condition. Furthermore, we had previously analyzed the space-time profiles of SOs in the same data with same referencing approach and found no lateralization effect in those oscillations. Hence, we interpret the Frontal-Right and Left clusters as data-driven and emerging from the high variability of spindle space-time profiles. Functionally, we hypothesize that these non-symmetrical spindles could be linked to the lateral nature of numerous cognitive and perceptual processes, since spindles are hypothesized to promote consolidation by modulating coordinated activity that is directly linked to awake encoding activity ("reactivation", or "replay").

When we compared how many spindles were participating in each cluster type in each sleep stage (Figure 3B), we found that the relative majority of spindles in our dataset (about 35-40% of all spindles) was Local, while only about 10% of all spindles were Global. In comparing spindle cluster participation across the two NREM sleep stages, we found that there was a larger fraction of Global spindles in S2 compared to SWS, and vice versa, slightly more Local spindles in SWS compared to S2 (this was also true for Posterior spindles). (Statistical analysis found an effect of cluster type and cluster-by-sleep stage interaction,

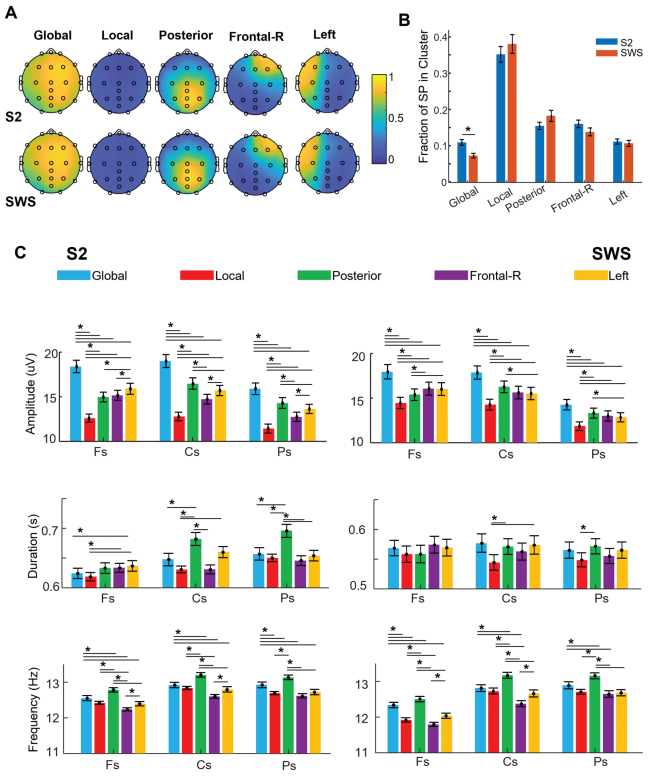

Figure 3. Topographical clustering of co-occurring spindles. (A) Topoplots showing the average of detection electrode locations for spindles in each of the clusters, separating spindles in Global, Local, Posterior, Frontal-Right, and Left. (B) Fraction of spindles in a given cluster. Note that the majority of spindles is Local in both sleep stages. (C) Properties of spindles across clusters and three main electrode regions: Frontal (F), Central (C), and Parietal (P). Plots on the left show results for S2 spindles, on the right for SWS spindles. At each region, bars of different colors represent the average value of the property for spindles in one cluster: Global (blue), Local (red), Posterior (green), Frontal-Right (Purple), and Left (yellow). Error-bars mark s.e.m. across subjects. Top row: spindle amplitude (in uV), middle row: duration (in s), bottom row: frequency (in Hz).

but not sleep stage, with post-hoc analysis confirming the difference in fraction of Global spindles in S2 vs SWS, but not for other spindle clusters).

We then tested if topographical clustering of spindles could differentiate spindle occurrences that had different properties. We compared basic spindle properties (amplitude, duration, and frequency) across locations on the electrode manifold (frontal, central and parietal) in spindles in different clusters (Figure 3C). The same properties at FP and O locations are shown in Supplementary Figure S5.

The top plots in Figure 3C show that Global spindles had the largest amplitude of all clusters in both sleep stages at all locations. Conversely, Local spindles showed smallest amplitude at all locations in both sleep stages. This is consistent with an effect of amplitude on spindle co-detection in the EEG, where at the extremes of amplitude range (largest and smallest) the Global and Local cluster capture spindles space-time profiles. The other three spindle clusters had intermediate amplitudes, with Posterior spindles relatively smaller at F electrodes and larger at C-P electrodes in both stages. (In both sleep stages, statistical analysis found an effect of cluster type and cluster-by-electrode interaction, but not electrode. Post-hoc analysis in S2 confirming the difference in spindle amplitude across clusters within each electrode. Post-hoc analysis in SWS confirming the difference in spindle amplitude across clusters within each electrode). Of note, specific amplitude value ranges of individual spindles in different clusters were not drastically different (Supplementary Figure S6), suggesting that amplitude was not the dominant factor differentiating co-detection profiles of spindles.

The middle plots in Figure 3C compare the duration of spindles in different clusters. During S2, Posterior spindles showed longer durations than spindles in Global, Local and Frontal clusters at C and P electrodes. (Statistical analysis found an effect of cluster type, electrode, and interaction; with post-hoc analysis confirming the longer duration of Posterior spindles). During SWS, spindle duration was very similar across clusters. (Statistical analysis found no effect of cluster type, electrode, or interaction; with post-hoc analysis confirming very few differences in spindle duration across clusters within each electrode location).

The bottom plots in Figure 3C compare the frequency of spindles in different clusters. During both S2 and SWS, spindles in different clusters showed different average frequency at all locations, with Posterior spindles showing the faster average frequency and Fronto-Right spindles showing the slowest average frequency across clusters. (Statistical analysis within S2 found an effect of cluster type and electrode, but not interaction; with post-hoc analysis confirming the difference in frequency of spindles across clusters within the same electrode location. Statistical analysis within SWS found an effect of cluster type, electrode, and interaction; with post-hoc analysis confirming the difference in frequency of spindles across clusters within the same electrode location).

In summary, our data show that in both stages Global spindles had larger amplitudes than all other spindle types, but no specific duration or frequency distinction characterized this cluster further. Conversely, Local spindles showed amplitudes smaller than spindles in all other clusters and no further distinction in frequency or duration. Among the other three spindle clusters that have specific topographies (Posterior, Frontal-Right, and Left), there was an evident differentiation for Posterior spindles: in both stages, they showed a faster average frequency at all locations, and in S2, they were also longer than other spindles at centro-posterior locations. Conversely, Fronto-Right spindles showed lower average frequency at all locations. Hence, we interpret the Posterior spindle cluster as identifying those spindles that have been categorized as "fast spindles" [42, 66, 67, 74], commonly considered to occur at parietal locations. We also interpret Fronto-Right spindles as encompassing the classic "slow spindles", expected to occur at frontal locations.

Non-uniform participation of spindle space-time profiles in SO-spindle complexes

Since we found that spindles organize in five different topographical types, we asked if any of these types were especially likely to participate in a spindle-SO complex. In Figure 4, we present these results as percent sample probability over all complexes found in S2 or SWS, separately. For simplicity, we show our results for SO-SP* complexes in S2 and SWS only (the analogous figure for SP*-SO complexes is available as Supplementary Figure S6). In any given SO-SP* complex, the SO can be of one of three topographical types (Global, Local or Frontal) and the spindle can be one of five: Global, Local, Posterior, Frontal-Right, or Left. Each bar plot shows a specific SO-SP* type, based on its line (SO type) and column (spindle type) placement, comparing S2 (blue) and SWS (orange). The height of the bar plot is the average (across subjects) percent fraction of SO-SP* complexes of that type (at that location, in that sleep stage) compared to the total number of SO-SP* complexes found in the sleep stage. In the rightmost column, we show the fraction of SO-SP* types differentiating only among SO types but ignoring spindle type. Vice-versa, in the bottom line, we show the fraction of SO-SP* complexes differentiating only by spindle type but not SO type. As shown in Figure 4, the most frequent SO-SP* complex type in our data was a Global SO trough that precedes a Posterior spindle during SWS. This is consistent with our previous results (Figure 2), where the total available percent of spindles in SO-SP* complexes is larger in SWS than S2. One can also see that, regardless of SO type, Local spindles are more frequently found at frontal locations, while Posterior spindles participate most often in SO-SP* complexes at central locations. Conversely, if looking at SO types regardless of spindle type, Global SOs during SWS are most often participating in SO-SP* complexes, with no particular location preference. Since there are 15 possible topographical types of SO-SP* complexes and 5 possible electrode locations within each sleep stage, uniform distribution of SO-SP* types (i.e. if all types had the same chance to be found) would be at about 1.3%. Note that the complex of Global SO followed by a Posterior spindle at central electrodes during SWS is found about in 6% of all SO-SP* complexes in SWS, about five times higher than the uniform chance rate.

Discussion

In this work, we studied the structural properties and space-time profiles of spindles as events on the electrode manifold during overnight sleep in 34 adult volunteers, considering S2 and SWS separately. After detecting spindles based on their frequency-time profile [61], we studied their basic properties (frequency, amplitude, duration, and density) on the

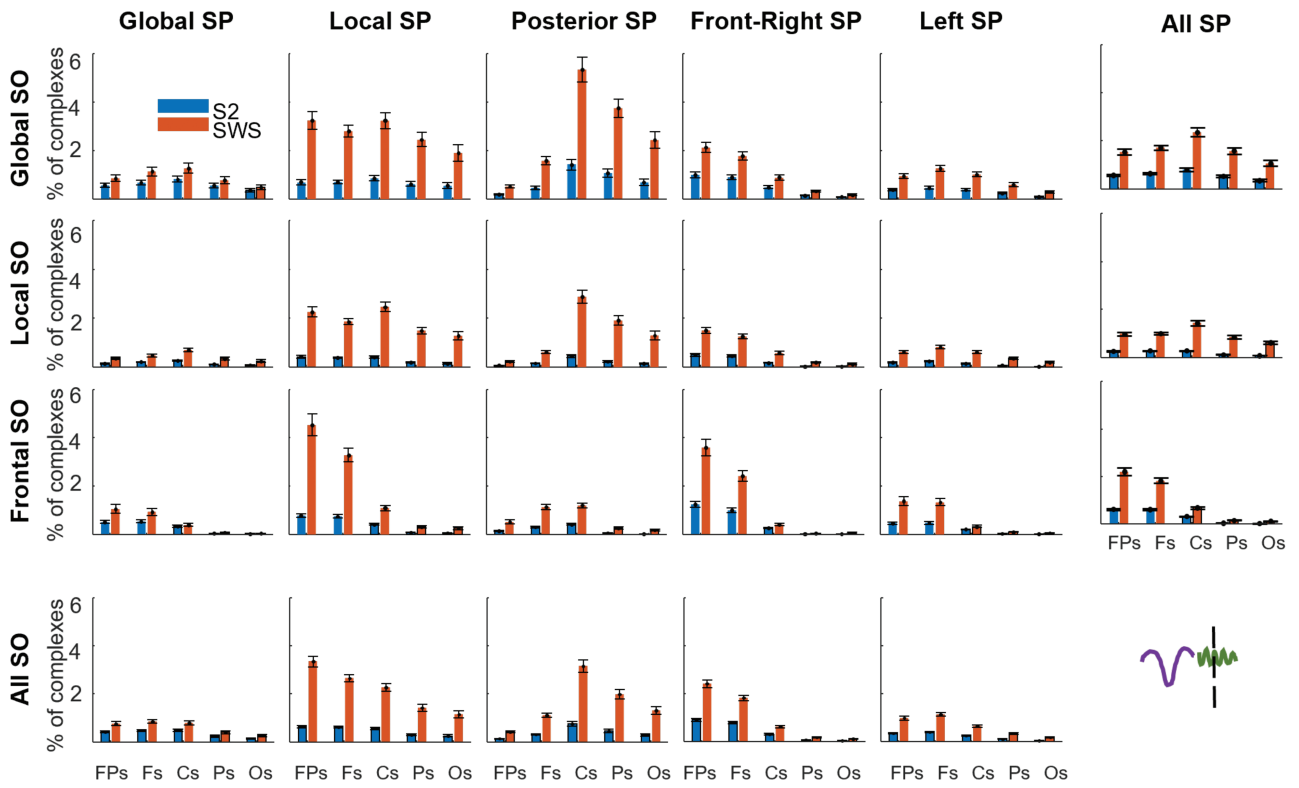

Figure 4. Topographical profile of the SO-SP* complexes. Plots show the fraction of all SO-SP* complexes of any given type, determined by counting the SO-SP* of each type in a given sleep stage and then dividing that value by the total number of SO-SP* complexes found in the sleep stage (error bars mark the SEM across subjects). In any given SO-SP* complex, the SO can be of one of three topographical types (Global, Local or Frontal – vertical axis) and the spindle can be one of five: Global, Local, Posterior, Frontal-Right, or Left (organized horizontally). We differentiate among electrode locations and compare S2 (blue bars) to SWS (orange bars). The right column shows the fraction of SO-SP* types based only on SO types. The bottom line shows the fraction of SO-SP* complexes differentiating by spindle type.

electrode manifold, and their time-coordination with SOs. We then applied our clustering approach to the characterization of spindle space-time profiles and finally describe the SO-spindle complexes in terms of the space-time properties of both SOs (introduced before [60]) and spindles (found in this work).

On the topography of spindle basic properties, we found—in both stages—a gradual acceleration of average spindle frequency from frontal to occipital locations, with SWS spindles at frontal electrodes slower (lower frequency) than S2 spindles. Average spindle duration was longer in S2 vs SWS. This suggests that while spindle properties show a large variance regardless of the sleep stage in which they are detected, there is a difference between S2 and SWS spindles. Of note, the faster parietal spindle frequency compared to frontal spindles is consistent with common terminology that identifies two types of spindles, fast and slow, with the fast spindles appearing posteriorly and slow spindles frontally. Still, in each electrode, we found spindles of all frequencies (10–16 Hz) and the average spindle frequency accelerated only of about 1 Hz from frontal to occipital electrodes. This has implication for spindle detection strategies, where the choice of pre-emptively isolating slow or fast spindle frequencies with pre-detection filtering would result in interfering with spindle shape and overall detection ability. Selection of spindles of the frequency of interest should instead be performed after detection.

When studying the interaction of SOs and spindles, we focused on complexes of one SO and one spindle, detected at the same electrode location within a 1-second delay. We found that the majority of SOs and spindles do not happen in temporal coordination with one another, rather a minority of them organize in SO-spindle complexes that involve spindles of faster frequencies landing after the down-to-up transition of the SO, about 500 ms after the SO trough. The time selectivity of the SO-spindle coordination is in agreement with numerous results [17–20, 73, 75, 76]. However, we also found that spindles involved in SO-spindle complexes show a frequency characterization narrower than the overall sigma range, biased toward a faster sigma rhythm [76]. This characterization of spindles that coordinate with SOs suggests that eliciting an SO-spindle complex in the cortical network is not necessarily given by promoting only the temporal coordination of the same SO initiation and spindle initiation that are involved in uncoupled events. Our data suggest that SO-SP* complexes could emerge as a space-time coordination phenomenon that results in SOs with large amplitudes and extensive propagation preceding faster spindles with shorter duration and larger amplitude emerging at posterior locations.

Current evidence does not allow for differentiation of the two cases, whether SO-spindle complexes emerge as part of a continuum or as separate, selected, events. In fact, pathways for coupled and uncoupled SOs and spindles can be found, since deafferented cortex can generate SOs in isolation [77], spindles are thalamic rhythms [36, 78], and cortical spindles involve thalamo-cortical and cortico-cortical interactions [37, 38, 79]. Hence, it is possible that an SO-spindle complex may arise

when a "trigger" event (e.g. a preceding theta oscillation [73]) recruits both an SO and a spindle generator, precipitating events that lead to a cortical SO-spindle complex. In such a model, for the spindles that participate in complexes to show faster frequencies, one would need the "trigger" mechanism to preferentially induce fast thalamic spindles, rather than spindles of any frequency. Such bias and dependence on a separate "initiating trigger" would imply that SO-spindle complexes are dynamical objects different from isolated SOs and isolated spindles, with specific timing and frequencies that enable appropriate cortical-subcortical communication. In this interpretation, the SO-spindle complex is a time-frequency "package" that imposes appropriate co-activation in regions that are exchanging information, and activated only in an information processing capacity. On the other hand, a contrasting model is that the SO-spindle complex could be generated as part of a continuum of SOs and spindles, mediated in their emergent properties (frequency, amplitude, and density) by the fine tuning of synaptic connections that change with encoding and consolidation. In this framework, a SO-spindle complex could emerge stochastically without relying on trigger events. Further research is needed to resolve these competing hypotheses.

When applying our clustering co-detection method to spindles, we found that the large variability in spindle properties was reflected in their topography, where five separate clusters were necessary to capture the different spindle profiles on the electrode manifold. We found that a relative majority (35%–40%) of spindles are Local, meaning they are co-detected on few electrodes, and in no specific location, while sizeable minorities (10%–20%) of spindles can be topographically characterized as Global, Posterior, Frontal-Right, and Left. Of note, Global spindles are larger, and Local spindles are smaller, than spindles in all other clusters at all locations. Posterior spindles last longer than other spindles at central and posterior locations in S2 but not in SWS, they are also faster than other spindles at central and posterior locations in both sleep stages. A number of studies have emphasized a potential link between the topography of cognitive daytime activity and topography of brain rhythms in the following sleep epoch [80, 81], and spindle topography could be strongly influenced by this mechanism. In particular the two spindle clusters that show hemispheric a-symmetry (Frontal-Right and Left spindles) could be representative of cognitive processes during sleep that are dependent on lateralized brain activity during the day (such as learning). Indeed, lateralized perceptual training induced retinotopically specific increases in sigma activity that was correlated with the magnitude of post-sleep performance improvement [81], underscoring the highly localized nature of spindle related processing. Consistent with our idea that oscillation space-time profiles are as important as relative timing, we found which types of SOs and spindles were more likely to appear in a SO-spindle complex. Clustering showed that the most common type of complex involved a Global SO preceding a Posterior spindle. Global SOs are larger than average SOs, showing a fronto-occipital travelling profile [60]. Posterior spindles are faster than other spindles at centro-parietal electrodes (Figure 3). As a result, our data suggest that the hypothesized mechanism of coordinated SOs and spindles during memory reactivation to mediate synaptic plasticity could be refined to concentrate on SOs of particularly large amplitude at the trough and spindles of faster frequency, and focusing on the dynamics at central and parietal electrodes.

Our core findings that spindle properties are different in SWS vs S2 sleep, that the minority of spindles that participate in SO-spindle complexes have different properties than uncoupled spindles, and that there is a non-uniform participation of spindle space-time profiles in SO-spindle paint a picture that has functional implications. Combined, our observations suggest that spindle generation is a layered phenomenon, where thalamic pacing and cortico-thalamic entrainment (necessary and sufficient for a spindle to emerge in cortical signal) are modulated by the neurochemistry of sleep stages and the timing in relation to SO activity, leading to the overall different properties of spindles in S2 vs SWS, and in coupled vs uncoupled spindles. Furthermore, the clustering result showing that space-time patterning of spindles is relevant to their presence in SO-SP complexes suggest that to elicit an SO-SP complex the network could be using a "trigger" different than those that lead to the emergence of uncoupled spindles.

Sleep neuroscience has long discussed potentially different roles for local vs global sleep dynamics in memory processing [82, 83] In particular, one recent theory by Genzel and colleagues [84] suggests that both global and local memory reactivations (mediated by localized and widespread brain events, respectively) might be participating in sleep-dependent consolidation, with light sleep (S2) enabling global reorganization of specific learning-related connections, and deep SO-rich sleep (SWS) mediating localized reorganization of connections via homeostatic regulation. In our data, when comparing spindle clusters in S2 vs SWS, we confirmed this dichotomy of increased "globality" of brain rhythms during S2 and increased "locality" of the same dynamics during SWS [60], with statistically more abundant Global spindles in S2 compared to SWS, and vice-versa a smaller fraction of Local spindles in S2 vs SWS (trend level). Functional implications of this layered structure of spindles and SO-spindle complexes in their space-time profiles expand beyond their role in memory consolidation. While our algorithmic approach to space-time detection of sleep rhythms profiles is a step removed from current clinical sleep settings, our data-driven approach can reveal structural properties of spindle space-time patterns that can be different in clinical populations, for example in those with generalized epilepsies that are thalamic-driven [85, 86]. Greater understanding of the space-time profiles of spindles may contribute to revealing mechanisms underlying a wide range of functions and interventions, including targeting specific memories for reinforcement [62, 87] or deletion [88]; developmental changes [56, 89] and clinical conditions [90–93]; attentional processes [94], as well as indicators of consciousness [95], and as factors contrasting sleep fragility [96, 97].

Supplementary Material

Supplementary material is available at *SLEEP* online.

Funding

Sleep data collection was supported by National Institute of Health: Grant (R01 AG046646) to SCM.

Disclosure Statement

None declared.

References

1. Roopun AK, *et al*. Temporal interactions between cortical rhythms. *Front Neurosci*. 2008;**2**(2):145–154. doi:10.3389/neuro.01.034.2008
2. Steriade M. Grouping of brain rhythms in corticothalamic systems. *Neuroscience*. 2006;**137**(4):1087–1106. doi:10.1016/j.neuroscience.2005.10.029
3. Buzsaki G, *et al*. Scaling brain size, keeping timing: evolutionary preservation of brain rhythms. *Neuron*. 2013;**80**(3):751–764.
4. Thut G, *et al*. The functional importance of rhythmic activity in the brain. *Curr Biol*. 2012;**22**(16):R658–R663.
5. Kopell N, *et al*. Are different rhythms good for different functions? *Front Hum Neurosci*. 2010;**4**:187. doi:10.3389/fnhum.2010.00187.
6. Csicsvari J, *et al*. Oscillatory coupling of hippocampal pyramidal cells and interneurons in the behaving Rat. *J Neurosci*. 1999;**19**(1):274–287.
7. Tort AB, *et al*. Theta-gamma coupling increases during the learning of item-context associations. *Proc Natl Acad Sci USA*. 2009;**106**(49):20942–20947.
8. Lee H, *et al*. Phase locking of single neuron activity to theta oscillations during working memory in monkey extrastriate visual cortex. *Neuron*. 2005;**45**(1):147–156.
9. Girardeau G, *et al*. Hippocampal ripples and memory consolidation. *Curr Opin Neurobiol*. 2011;**21**(3):452–459.
10. Sadowski JH, *et al*. Ripples make waves: binding structured activity and plasticity in hippocampal networks. *Neural Plast*. 2011;**2011**:960389.
11. Dickey CW, *et al*. Travelling spindles create necessary conditions for spike-timing-dependent plasticity in humans. *Nat Commun*. 2021;**12**(1):1027. doi:10.1038/s41467-021-21298-x.
12. Timofeev I, *et al*. Sleep slow oscillation and plasticity. *Curr Opin Neurobiol*. 2017;**44**:116–126.
13. Massimini M, *et al*. The sleep slow oscillation as a traveling wave. *J Neurosci*. 2004;**24**(31):6862–6870.
14. Contreras D, *et al*. Spatiotemporal patterns of spindle oscillations in cortex and thalamus. *J Neurosci*. 1997;**17**(3):1179–1196.
15. Dimitrov T, *et al*. Sleep spindles comprise a subset of a broader class of electroencephalogram events. *Sleep*. 2021;**44**(9). doi:10.1093/sleep/zsab099
16. Buzsaki G. Hippocampal sharp wave-ripple: a cognitive biomarker for episodic memory and planning. *Hippocampus*. 2015;**25**(10):1073–1188.
17. Molle M, *et al*. Slow oscillations orchestrating fast oscillations and memory consolidation. *Prog Brain Res*. 2011;**193**:93–110.
18. Latchoumane CV, *et al*. Thalamic spindles promote memory formation during sleep through triple phase-locking of cortical, thalamic, and hippocampal rhythms. *Neuron*. 2017;**95**(2):424–435 e426.
19. Sirota A, *et al*. Communication between neocortex and hippocampus during sleep in rodents. *Proc Natl Acad Sci USA*. 2003;**100**(4):2065–2069.
20. Staresina BP, *et al*. Hierarchical nesting of slow oscillations, spindles and ripples in the human hippocampus during sleep. *Nat Neurosci*. 2015;**18**(11):1679–1686.
21. Yamadori A. Role of the spindles in the onset of sleep. *Kobe J Med Sci*. 1971;**17**(3):97–111.
22. Tononi G, *et al*. Sleep function and synaptic homeostasis. *Sleep Med Rev*. 2006;**10**(1):49–62.
23. Xie L, *et al*. Sleep drives metabolite clearance from the adult brain. *Science*. 2013;**342**(6156):373–377.
24. Mander BA, *et al*. Beta-amyloid disrupts human NREM slow waves and related hippocampus-dependent memory consolidation. *Nat Neurosci*. 2015;**18**(7):1051–1057.
25. Diekelmann S, *et al*. The memory function of sleep. *Nat Rev Neurosci*. 2010;**11**(2):114–126.
26. Klinzing JG, *et al*. Mechanisms of systems memory consolidation during sleep. *Nat Neurosci*. 2019;**22**(10):1598–1610.
27. Rasch B, *et al*. About sleep's role in memory. *Physiol Rev*. 2013;**93**(2):681–766.
28. Stickgold R, *et al*. Sleep-dependent memory consolidation and reconsolidation. *Sleep Med*. 2007;**8**(4):331–343.
29. Marshall L, *et al*. Boosting slow oscillations during sleep potentiates memory. *Nature*. 2006;**444**(7119):610–613.
30. Mednick SC, *et al*. The critical role of sleep spindles in hippocampal-dependent memory: a pharmacology study. *J Neurosci*. 2013;**33**(10):4494–4504.
31. Cellini N, *et al*. Short duration repetitive transcranial electrical stimulation during sleep enhances declarative memory of facts. *Front Hum Neurosci*. 2019;**13**:123. doi:10.3389/fnhum.2019.00123.
32. Ngo HV, *et al*. Auditory closed-loop stimulation of the sleep slow oscillation enhances memory. *Neuron*. 2013;**78**(3):545–553.
33. Lustenberger C, *et al*. Feedback-controlled transcranial alternating current stimulation reveals a functional role of sleep spindles in motor memory consolidation. *Curr Biol*. 2016;**26**(16):2127–2136.
34. McCormick DA, *et al*. Sleep and arousal: thalamocortical mechanisms. *Annu Rev Neurosci*. 1997;**20**:185–215.
35. Fuentealba P, *et al*. The reticular nucleus revisited: intrinsic and network properties of a thalamic pacemaker. *Prog Neurobiol*. 2005;**75**(2):125–141.
36. Bazhenov M, *et al*. Spiking-bursting activity in the thalamic reticular nucleus initiates sequences of spindle oscillations in thalamic networks. *J Neurophysiol*. 2000;**84**(2):1076–1087.
37. Bonjean M, *et al*. Corticothalamic feedback controls sleep spindle duration in vivo. *J Neurosci*. 2011;**31**(25):9124–9134.
38. Contreras D, *et al*. Control of spatiotemporal coherence of a thalamic oscillation by corticothalamic feedback. *Science*. 1996;**274**(5288):771–774.
39. Cox R, *et al*. Individual differences in frequency and topography of slow and fast sleep spindles. *bioRxiv preprint first posted online Mar 3, 2017*; 2017. https://doi.org/10.1101/113373
40. Piantoni G, *et al*. Spatiotemporal characteristics of sleep spindles depend on cortical location. *Neuroimage*. 2017;**146**:236–245.
41. Jobert M, *et al*. Topographical analysis of sleep spindle activity. *Neuropsychobiology*. 1992;**26**(4):210–217.
42. Zeitlhofer J, *et al*. Topographic distribution of sleep spindles in young healthy subjects. *J Sleep Res*. 1997;**6**(3):149–155.
43. Werth E, *et al*. Spindle frequency activity in the sleep EEG: individual differences and topographic distribution. *Electroencephalogr Clin Neurophysiol*. 1997;**103**(5):535–542.
44. Muller L, *et al*. Rotating waves during human sleep spindles organize global patterns of activity that repeat precisely through the night. *Elife*. 2016;**5**:e17267. doi:10.7554/eLife.17267
45. Krishnan GP, *et al*. Thalamocortical and intracortical laminar connectivity determines sleep spindle properties. *PLoS Comput Biol*. 2018;**14**(6):e1006171.
46. Dang-Vu TT, *et al*. Spontaneous brain rhythms predict sleep stability in the face of noise. *Curr Biol*. 2010;**20**(15):R626–R627.
47. Schabus M, *et al*. The fate of incoming stimuli during NREM sleep is determined by spindles and the phase of

the slow oscillation. *Front Neurol*. 2012;**3**:40. doi:10.3389/fneur.2012.00040.
48. Rudzik F, *et al*. Sleep spindle characteristics and arousability from nighttime transportation noise exposure in healthy young and older individuals. *Sleep*. 2018;**41**(7). doi:10.1093/sleep/zsy077
49. Zhang ZY, *et al*. Longitudinal analysis of sleep spindle maturation from childhood through late adolescence. *J Neurosci*. 2021;**41**(19):4253–4261.
50. Principe JC, *et al*. Sleep spindle characteristics as a function of age. *Sleep*. 1982;**5**(1):73–84.
51. Nicolas A, *et al*. Sleep spindle characteristics in healthy subjects of different age groups. *Clin Neurophysiol*. 2001;**112**(3):521–527.
52. Mander BA, *et al*. Sleep and human aging. *Neuron*. 2017;**94**(1):19–36.
53. Hoedlmoser K, *et al*. Slow sleep spindle activity, declarative memory, and general cognitive abilities in children. *Sleep*. 2014;**37**(9):1501–1512. doi:10.5665/sleep.4000
54. Geiger A, *et al*. The sleep EEG as a marker of intellectual ability in school age children. *Sleep*. 2011;**34**(2):181–189. doi:10.1093/sleep/34.2.181
55. Fogel SM, *et al*. Sleep spindles and learning potential. *Behav Neurosci*. 2007;**121**(1):1–10.
56. Schabus M, *et al*. Sleep spindle-related activity in the human EEG and its relation to general cognitive and learning abilities. *Eur J Neurosci*. 2006;**23**(7):1738–1746.
57. Sattari N, *et al*. The effect of sex and menstrual phase on memory formation during a nap. *Neurobiol Learn Mem*. 2017;**145**:119–128.
58. Baker FC, *et al*. Impact of sex steroids and reproductive stage on sleep-dependent memory consolidation in women. *Neurobiol Learn Mem*. 2019;**160**:118–131.. doi:10.1016/j.nlm.2018.03.017.
59. Baker FC, *et al*. Menstrual cycle effects on sleep. *Sleep Med Clin*. 2018;**13**(3):283–294.
60. Malerba P, *et al*. Spatio-temporal structure of sleep slow oscillations on the electrode manifold and its relation to spindles. *Sleep*. 2019;**42**(1). doi:10.1093/sleep/zsy197
61. Prerau MJ, *et al*. Sleep neurophysiological dynamics through the lens of multitaper spectral analysis. *Physiology (Bethesda)*. 2017;**32**(1):60–92.
62. Antony JW, *et al*. Sleep spindle refractoriness segregates periods of memory reactivation. *Curr Biol*. 2018;**28**(11):1736–1743 e1734.
63. Wamsley EJ, *et al*. Reduced sleep spindles and spindle coherence in schizophrenia: mechanisms of impaired memory consolidation? *Biol Psychiatry*. 2012;**71**(2):154–161.
64. Molle M, *et al*. Grouping of spindle activity during slow oscillations in human non-rapid eye movement sleep. *J Neurosci*. 2002;**22**(24):10941–10947.
65. Dang-Vu TT, *et al*. Spontaneous neural activity during human slow wave sleep. *Proc Natl Acad Sci USA*. 2008;**105**(39):15160–15165.
66. Molle M, *et al*. Fast and slow spindles during the sleep slow oscillation: disparate coalescence and engagement in memory processing. *Sleep*. 2011;**34**(10):1411–1421. doi:10.5665/SLEEP.1290
67. Klinzing JG, *et al*. Spindle activity phase-locked to sleep slow oscillations. *Neuroimage*. 2016;**134**:607–616.
68. McVea DA, *et al*. Large scale cortical functional networks associated with slow-wave and spindle-burst-related spontaneous activity. *Front Neural Circuits*. 2016;**10**:103.
69. Mikutta C, *et al*. Phase-amplitude coupling of sleep slow oscillatory and spindle activity correlates with overnight memory consolidation. *J Sleep Res*. 2019;**28**(6):e12835. doi:10.1111/jsr.12835.
70. Siapas AG, *et al*. Coordinated interactions between hippocampal ripples and cortical spindles during slow-wave sleep. *Neuron* 1998;**21**(5):1123–1128.
71. Wei Y, *et al*. Synaptic mechanisms of memory consolidation during sleep slow oscillations. *J Neurosci*. 2016;**36**(15):4231–4247.
72. Sanda P, *et al*. Bidirectional interaction of hippocampal ripples and cortical slow waves leads to coordinated spiking activity during NREM sleep. *Cereb Cortex*. 2021;**31**(1):324–340. doi:10.1093/cercor/bhaa228.
73. Gonzalez CE, *et al*. Theta bursts precede, and spindles follow, cortical and thalamic downstates in human NREM sleep. *J Neurosci*. 2018;**38**(46):9989–10001.
74. Finelli LA, *et al*. Functional topography of the human nonREM sleep electroencephalogram. *Eur J Neurosci*. 2001;**13**(12):2282–2290.
75. De Gennaro L, *et al*. An electroencephalographic fingerprint of human sleep. *Neuroimage*. 2005;**26**(1):114–122.
76. Cox R, *et al*. Large-scale structure and individual fingerprints of locally coupled sleep oscillations. *Sleep*. 2018;**41**(12). doi:10.1093/sleep/zsy175
77. Timofeev I, *et al*. Origin of slow cortical oscillations in deafferented cortical slabs. *Cereb Cortex*. 2000;**10**(12):1185–1199.
78. Grenier F, *et al*. Leading role of thalamic over cortical neurons during postinhibitory rebound excitation. *Proc Natl Acad Sci USA*. 1998;**95**(23):13929–13934.
79. Piantoni G, *et al*. The contribution of thalamocortical core and matrix pathways to sleep spindles. *Neural Plast*. 2016;**2016**:3024342.
80. Piantoni G, *et al*. Memory traces of long-range coordinated oscillations in the sleeping human brain. *Hum Brain Mapp*. 2015;**36**(1):67–84.
81. Bang JW, *et al*. Location specific sleep spindle activity in the early visual areas and perceptual learning. *Vision Res*. 2014;**99**:162–171.
82. Siclari F, *et al*. Local aspects of sleep and wakefulness. *Curr Opin Neurobiol*. 2017;**44**:222–227.
83. Bernardi G, *et al*. Local and widespread slow waves in stable NREM sleep: evidence for distinct regulation mechanisms. *Front Hum Neurosci*. 2018;**12**:248. doi:10.3389/fnhum.2018.00248.
84. Genzel L, *et al*. Light sleep versus slow wave sleep in memory consolidation: a question of global versus local processes? *Trends Neurosci*. 2014;**37**(1):10–19.
85. Bagshaw AP, *et al*. Sleep onset uncovers thalamic abnormalities in patients with idiopathic generalised epilepsy. *Neuroimage Clin*. 2017;**16**:52–57.
86. Spencer ER, *et al*. Source EEG reveals that Rolandic epilepsy is a regional epileptic encephalopathy. *Neuroimage Clin*. 2022;**33**:102956.
87. Antony JW, *et al*. Cued memory reactivation during sleep influences skill learning. *Nat Neurosci*. 2012;**15**(8):1114–1116.
88. Carbone J, *et al*. The effect of zolpidem on targeted memory reactivation during sleep. *Learn Mem*. 2021;**28**(9):307–318.
89. Hahn M, *et al*. Developmental changes of sleep spindles and their impact on sleep-dependent memory consolidation and general cognitive abilities: a longitudinal approach. *Dev Sci*. 2019;**22**(1):e12706.
90. Ferrarelli F, *et al*. Thalamic dysfunction in schizophrenia suggested by whole-night deficits in slow and fast spindles. *Am J Psychiatry*. 2010;**167**(11):1339–1348.
91. Smith FRH, *et al*. Consolidation of vocabulary is associated with sleep in typically developing children, but not in children with dyslexia. *Dev Sci*. 2018;**21**(5):e12639.

92. Tessier S, *et al*. Intelligence measures and stage 2 sleep in typically-developing and autistic children. *Int J Psychophysiol*. 2015;**97**(1):58–65.
93. Prehn-Kristensen A, *et al*. Reduced sleep-associated consolidation of declarative memory in attention-deficit/hyperactivity disorder. *Sleep Med*. 2011;**12**(7):672–679.
94. Cellini N, *et al*. Sleep after practice reduces the attentional blink. *Atten Percept Psychophys*. 2015;**77**(6):1945–1954.
95. Pan J, *et al*. A systematic review of sleep in patients with disorders of consciousness: from diagnosis to prognosis. *Brain Sci*. 2021;**11**(8):1072. doi:10.3390/brainsci11081072.
96. De Gennaro L, *et al*. Sleep spindles: an overview. *Sleep Med Rev*. 2003;**7**(5):423–440.
97. Benbir Senel G, *et al*. Changes in sleep structure and sleep spindles are associated with the neuropsychiatric profile in paradoxical insomnia. *Int J Psychophysiol*. 2021;**168**:27–32.